
The Rise of AI Language Pathologists: Exploring Two-level Prompt Learning for Few-shot Weakly-supervised Whole Slide Image Classification

Linhao Qu^{1,2}, Xiaoyuan Luo^{1,2}, Kexue Fu^{1,2}, Manning Wang^{*1,2}, Zhijian Song^{*1,2}

¹Digital Medical Research Center, School of Basic Medical Science, Fudan University.

²Shanghai Key Lab of Medical Image Computing and Computer Assisted Intervention.

Abstract

This paper introduces the novel concept of few-shot weakly supervised learning for pathology Whole Slide Image (WSI) classification, denoted as FSWC. A solution is proposed based on prompt learning and the utilization of a large language model, GPT-4. Since a WSI is too large and needs to be divided into patches for processing, WSI classification is commonly approached as a Multiple Instance Learning (MIL) problem. In this context, each WSI is considered a bag, and the obtained patches are treated as instances. The objective of FSWC is to classify both bags and instances with only a limited number of labeled bags. Unlike conventional few-shot learning problems, FSWC poses additional challenges due to its weak bag labels within the MIL framework. Drawing inspiration from the recent achievements of vision-language models (V-L models) in downstream few-shot classification tasks, we propose a two-level prompt learning MIL framework tailored for pathology, incorporating language prior knowledge. Specifically, we leverage CLIP to extract instance features for each patch, and introduce a prompt-guided pooling strategy to aggregate these instance features into a bag feature. Subsequently, we employ a small number of labeled bags to facilitate few-shot prompt learning based on the bag features. Our approach incorporates the utilization of GPT-4 in a question-and-answer mode to obtain language prior knowledge at both the instance and bag levels, which are then integrated into the instance and bag level language prompts. Additionally, a learnable component of the language prompts is trained using the available few-shot labeled data. We conduct extensive experiments on three real WSI datasets encompassing breast cancer, lung cancer, and cervical cancer, demonstrating the notable performance of the proposed method in bag and instance classification. All codes will be made publicly accessible at <https://github.com/miccaiif/TOP>.

1 Introduction

The automated analysis of pathology Whole Slide Images (WSIs) plays a crucial role in contemporary cancer diagnosis and the prediction of treatment response [25, 33, 21, 23, 19]. Unlike natural images, WSIs typically possess a gigapixel resolution, rendering them unsuitable as direct inputs for deep learning models. To address this problem, a common approach involves dividing WSIs into non-overlapping small patches for subsequent processing. However, due to the vast number of patches within a single WSI, it is impractical to assign fine-grained labels to these small patches, rendering instance-level supervised methods unfeasible [29, 8, 6, 20, 22]. Consequently, Multiple Instance Learning (MIL), a popular weakly supervised learning paradigm, has emerged as an effective solution

*Corresponding Authors.

to overcome these challenges. In the MIL framework, each WSI is considered a "bag", and the extracted patches are regarded as instances within this bag. In a positive bag, there exists at least one positive instance, while in a negative bag, all instances are negative. During training, only the bag labels are known, whereas the instance labels remain unknown [26, 38]. Deep learning-based WSI classification typically involves two tasks: bag-level classification, accurately predicting the category of the target bag, and instance-level classification, accurately identifying positive instances within positively labeled bags.

MIL methods for WSI classification can be broadly categorized into instance-based methods [3, 9, 26, 17] and bag-based methods [13, 31, 16, 41, 30, 7, 22, 37, 35]. Instance-based approaches involve training an instance classifier using artificially-generated pseudo labels to estimate the probability of each instance being positive. These individual predictions are then aggregated to obtain the bag-level prediction. On the other hand, bag-based methods have emerged as the predominant approach for WSI classification. These methods initially extract features for each instance and subsequently employ an aggregation function to combine the features of all instances within a bag into a single bag feature. Finally, a bag classifier is trained using the known labels of the bags. Recently, attention-based aggregation methods [13, 12, 43, 39, 31, 16, 41, 22] have demonstrated promising performance, and they could leverage attention scores assigned to each instance for instance-level classification.

Most existing MIL methods for WSI classification assume the availability of a substantial amount of labeled data at the bag level. However, in clinical practice, limitations such as patient privacy concerns, challenges in obtaining pathological samples, or the diagnosis of rare or emerging diseases often result in a scarcity of pathological data [25, 33, 29, 8, 15]. Consequently, existing methods are ill-equipped to handle such few-shot learning scenarios. In this paper, **we present a novel WSI classification problem termed Few-shot Weakly Supervised WSI Classification (FSWC)**. Traditional few-shot learning strives to achieve good classification performance with very few labeled support samples per class (usually only 1, 2, 4, 8, or 16 samples). Similarly, in FSWC, only a few bags are labeled for training (only 1, 2, 4, 8, or 16 per class). Notably, FSWC diverges from traditional few-shot learning on natural images due to the absence of instance-level labels, with only bag-level labels provided. The MIL setting and the absence of instance labels make FSWC considerably more challenging than traditional few-shot learning problems. **The primary objective of FSWC is to achieve precise bag-level and instance-level classification with very few training bags.** Figure 1 A and B provide intuitive illustrations of the existing WSI classification and FSWC tasks.

Recently, significant advancements have been made in visual representation and transfer learning with the emergence of vision-language models (V-L models) such as CLIP [28], ALIGN [14], and FLIP [40]. These models have demonstrated remarkable success, indicating their ability to learn universal visual representations and perform effectively in zero-shot or few-shot settings for downstream tasks. **Motivated by these achievements, we apply V-L models to address the FSWC problem.** Unlike traditional visual frameworks, V-L models employ a two-tower architecture consisting of an Image Encoder and a Text Encoder for pre-training on extensive image-text pairs. The objective is to align images and their corresponding description texts within a shared feature space. For zero-shot classification tasks, a carefully designed prompt template, such as "a photo of a [CLS]," is utilized to classify the target image through similarity matching in the corresponding feature space. To enhance transfer performance and eliminate the need for handcrafted prompt templates, methods like CoOp [42] replace manual prompts with learned prompt representations. These approaches adapt V-L models for few-shot image recognition tasks using a small number of labeled images from the target dataset, with only prompt parameters being trained while the V-L model parameters remain fixed. Figure 1 C provides an intuitive depiction of the fine-tuning paradigm based on pre-trained V-L models and prompt learning in the context of natural images. A straightforward application of V-L models in FSWC involves using the Image Encoder to extract instance features within each bag and aggregating these instance features into bag-level representations using established aggregation functions. Subsequently, prompt learning algorithms like CoOp [42] can be employed at the bag level. However, our experimental results demonstrate unsatisfactory performance with this approach. **The main challenges lie in the absence of efficient instance aggregation methods and the complexity of designing appropriate bag-level prompts.**

In order to effectively utilize V-L models for addressing the FSWC problem, we present a **Two-level Prompt Learning MIL framework** guided by pathology language prior knowledge, referred to as **TOP**. The main concept of TOP is illustrated in Figure 1 D. Initially, we employ the Image Encoder of V-L models to extract instance features within each bag. Subsequently, we introduce prompt guided

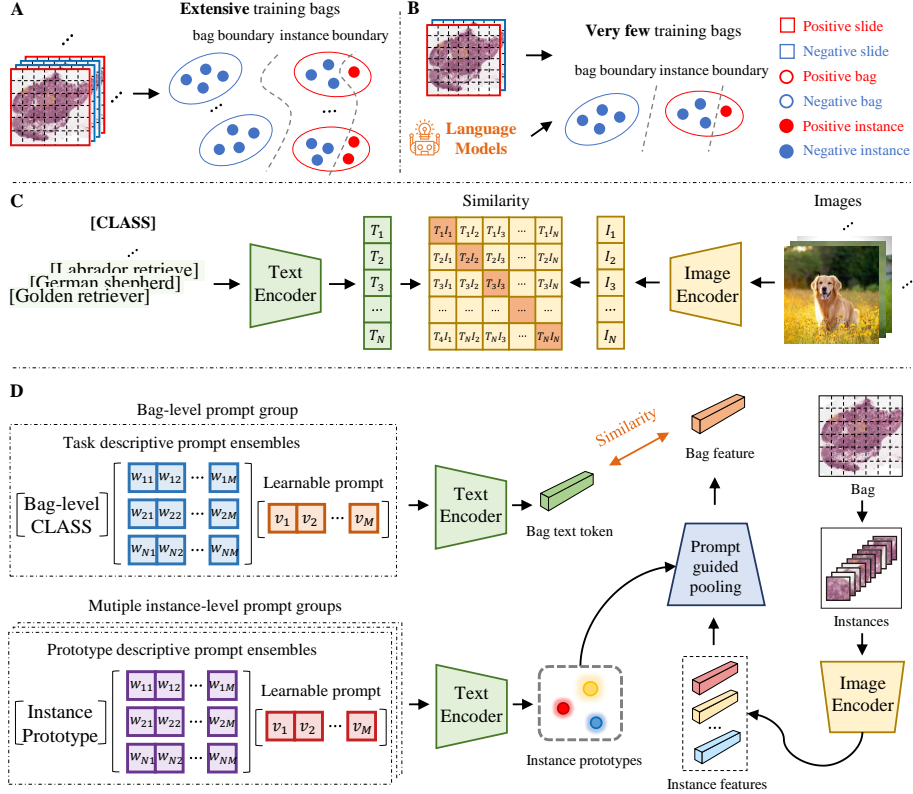


Figure 1: A. Existing WSI classification tasks. B. Our proposed FSWC task based on language models. C. Existing prompt learning paradigm using pre-trained V-L models, where the parameters of the V-L models are always frozen. D. Our proposed Two-level Prompt Learning paradigm.

pooling as a means to aggregate these instance features into a bag-level feature. To facilitate this aggregation process, we leverage the capabilities of the large language model GPT-4 [24] to generate multiple instance-level prompt groups. These prompt groups serve as instance-level pathology language prior knowledge, effectively guiding the aggregation process. Furthermore, GPT-4 [24] is utilized to construct a bag-level prompt group, which is matched with the bag feature to facilitate few-shot prompt learning at the bag level. Throughout this process, the bag-level prompt group acts as pathology language prior knowledge, providing guidance for the few-shot prompt learning process. In TOP, both the instance-level and bag-level prompts comprise three components. The first component encompasses the task label at the instance or bag level, such as "an image patch of [Lymphocytes]" and "a WSI of [Lung adenocarcinoma]." The second component consists of a combination of various visual description texts associated with the given task label. It is important to note that these visual descriptions are not manually designed, but are obtained through a question-answering approach employing GPT-4. For example, we generate prompts such as "What are the visual pathological forms of Lung adenocarcinoma?". Our experimental findings consistently demonstrate the criticality of incorporating task-specific visual descriptions tailored to the pathological WSI classification task. Inspired by CoOp [42], we design the third component as a learnable continuous prompt representation, enabling automatic adaptation and further enhancing transfer performance.

The main contributions of this paper are as follows:

- We proposed and effectively solved the novel Few-shot Weakly Supervised WSI Classification (FSWC) problem.
- We propose a Two-level Prompt Learning MIL framework, referred to as TOP. At the instance level, we leverage pathology language prior knowledge derived from GPT-4 to guide the aggregation of instance features into bag features. In addition, at the bag level, we create a comprehensive bag-level prompt group by incorporating bag-level pathology categories and visual pathology descriptions as prior knowledge to facilitate few-shot learning under the supervision of bag labels.

- We conducted comprehensive evaluations on three real-world WSI datasets, including breast cancer, lung cancer, and cervical cancer. TOP demonstrates strong bag classification and instance classification performance under limited bag-level labeled data, achieving state-of-the-art results.

2 Related Work

2.1 Multiple Instance Learning for WSI Classification

Most MIL methods for WSI classification [13, 39, 31, 16, 41, 30, 7, 37, 18, 35] follow a two-step process: they extract features for each instance and then aggregate these instance features to obtain a representative bag feature. Subsequently, a bag classifier is trained using the bag features and corresponding labels. Notably, attention-based aggregation methods [13, 12, 43, 39, 31, 16, 41, 22] have demonstrated promising results, where attention scores assigned to each instance contribute to instance-level classification. However, these approaches heavily rely on a substantial number of labeled bags, which is not the case in our proposed FSWC task, where only a limited number of labeled bags are available for training. While some recent studies [16, 41, 30, 27, 4, 5] employed pre-trained networks to extract instance features, these models were solely pre-trained on self-supervised learning or ImageNet data. In contrast, we explore the utilization of pre-trained V-L models (as detailed in Section 2.3) for extracting instance features. Additionally, we present a Two-level Prompt Learning MIL framework guided by pathology language prior knowledge.

2.2 Few Shot Classification

The primary objective of Few-shot Classification (FSC) is to accurately classify test samples by utilizing limited labeled support examples. Typically, only 1, 2, 4, 8, or 16 examples per category are available. This classification process leverages learned knowledge and prior information [10, 11, 1, 32, 34, 36]. Recently, vision-language models (referred to as V-L models, detailed in Section 2.3) such as CLIP [28], ALIGN [14], and FLIP [40] have demonstrated significant success in FSC. This success suggests that these large models have acquired universal visual representations and exhibit improved performance in downstream tasks, particularly in zero-shot or few-shot scenarios. Nevertheless, the task of few-shot WSI classification under bag-level supervision has not yet been investigated. In this paper, we introduce this paradigm as few-shot weakly-supervised WSI classification (FSWC) and propose an effective solution by employing CLIP-based prompt learning.

2.3 Vision-language Models and Prompt Learning

Pre-trained Vision-Language (V-L) models, such as CLIP [28], ALIGN [14], and FLIP [40], which have been trained on extensive image-text pairs, exhibit remarkable potential in visual representation and transfer learning. These V-L models employ a dual-tower architecture that comprises visual and text encoders. They utilize contrastive learning to align text-to-image and image-to-text in the feature space. The pre-trained V-L models, including CLIP [28], demonstrate remarkable transferability in image recognition. By carefully designing text descriptions, referred to as "prompts," to align with the corresponding image features in the feature space, these models enable zero-shot or few-shot classification. Building on the accomplishments of CLIP, CoOp [42] replaces manually created prompts with a learned prompt representation and adapts V-L models to downstream FSC tasks. Motivated by the triumph of V-L models in FSC within the domain of natural images, we propose several techniques to effectively adapt pre-trained V-L models for addressing the FSWC problem.

3 Preliminaries

3.1 Problem Formulation

Given a dataset $X = \{X_1, X_2, \dots, X_N\}$ comprising N WSIs, and each WSI X_i is partitioned into non-overlapping small patches $\{x_{i,j}, j = 1, 2, \dots, n_i\}$, where n_i represents the number of patches obtained from X_i . All patches within X_i collectively form a bag, and each patch serves as an instance of that bag. The bag is assigned a label $Y_i \in \{0, 1\}$, where $i = \{1, 2, \dots, N\}$. The labels of each

instance $\{y_{i,j}, j = 1, 2, \dots, n_i\}$ are associated with the bag label in the following manner:

$$Y_i = \begin{cases} 0, & \text{if } \sum_j y_{i,j} = 0 \\ 1, & \text{else} \end{cases} \quad (1)$$

This implies that all instances within negative bags are assigned negative labels, whereas positive bags contain at least one positive-labeled instance. In the context of weakly-supervised MIL, only the bag label is provided for the training set, while the labels of individual instances remain unknown. The Few-shot Weakly-supervised WSI Classification (FSWC) task poses an even greater challenge as it allows for only a limited number of labeled bags for training. Typically, only a small number of bags per class, such as 1, 2, 4, 8, or 16, are available. The objective of FSWC is to accurately classify both the bags and individual instances, despite the scarcity of labeled training bags.

3.2 Vision-Language Pre-training and Few-shot Prompt Learning

We first provide a concise overview of the pre-training of V-L models and few-shot prompt learning. In this paper, we use the V-L model of CLIP [28], but our method is also applicable to other CLIP-like V-L models.

Model and Pre-training. The CLIP framework comprises an image encoder and a text encoder. The image encoder employs ResNet-50 or ViT to extract image features, while the text encoder uses Transformer to generate text features. CLIP’s primary training objective is to establish an embedding space that align image features with their corresponding text features by means of a contrastive loss. During training, a batch of image-text pairs is used, and CLIP maximizes the cosine similarity of matching pairs while minimizing the cosine similarity of all other non-matching pairs. To facilitate the acquisition of diverse visual concepts that can be readily applied to downstream tasks, CLIP is trained on a large-scale dataset consisting of 400 million image-text pairs, which includes medical data.

Zero-shot Inference. CLIP has the inherent ability to perform zero-shot classification because it is pre-trained to predict whether an image matches a given text description. Specifically, the approach involves using the image encoder to extract features from the image to be classified, using the text encoder to extract features of the text descriptions of all candidate categories (referred to as "prompts"), and then calculating the degree of match between the image features and all the text features to determine the classification category. Formally, let \mathbf{z} be the image feature extracted by the image encoder for image \mathbf{x} , and let $\{\mathbf{w}_i\}_{i=1}^K$ be a set of weight vectors generated by the text encoder. Here, K represents the number of candidate categories, and each \mathbf{w}_i comes from the prompt "a photo of a [CLASS]", where the CLASS token is replaced with a specific class name, such as "cat", "dog", or "car". The predicted probability of each category is calculated using Equation 2:

$$p(y = i | \mathbf{x}) = \frac{\exp(\cos(\mathbf{w}_i, \mathbf{f}) / \tau)}{\sum_{j=1}^K \exp(\cos(\mathbf{w}_j, \mathbf{f}) / \tau)} \quad (2)$$

Here, τ is the temperature coefficient learned by CLIP, and $\cos(\cdot, \cdot)$ represents cosine similarity.

Few-shot Prompt Learning. Research has shown that the construction of prompts plays a crucial role in the downstream task classification performance. CoOp [42] learns an end-to-end continuous vector as a supplementary prompt using limited labeled data from the downstream task. Formally, the overall prompt is designed as:

$$\mathbf{t} = [V]_1[V]_2 \dots [V]_M[CLASS] \quad (3)$$

where each $[V]_m (m \in \{1, \dots, M\})$ is a vector of the same dimension as the word embedding (i.e., 512 for CLIP), and M is a hyperparameter that specifies the number of context tokens. The text encoder of CLIP is used to encode the prompt \mathbf{t} to obtain a classification weight vector $\{\mathbf{w}_i\}_{i=1}^K$ that represents the visual concept, and then the prediction probability of each category is calculated according to Equation 2. A small amount of labeled data in the downstream task is used to train and optimize $[V]_m$ in the prompt using cross-entropy loss. Other parameters, including the Image Encoder and Text Encoder of the V-L model, are frozen.

$$\text{Loss} = CE(y, p) \quad (4)$$

where y represents the ground truth label and p represents the predicted probability of each class based on the prompt.

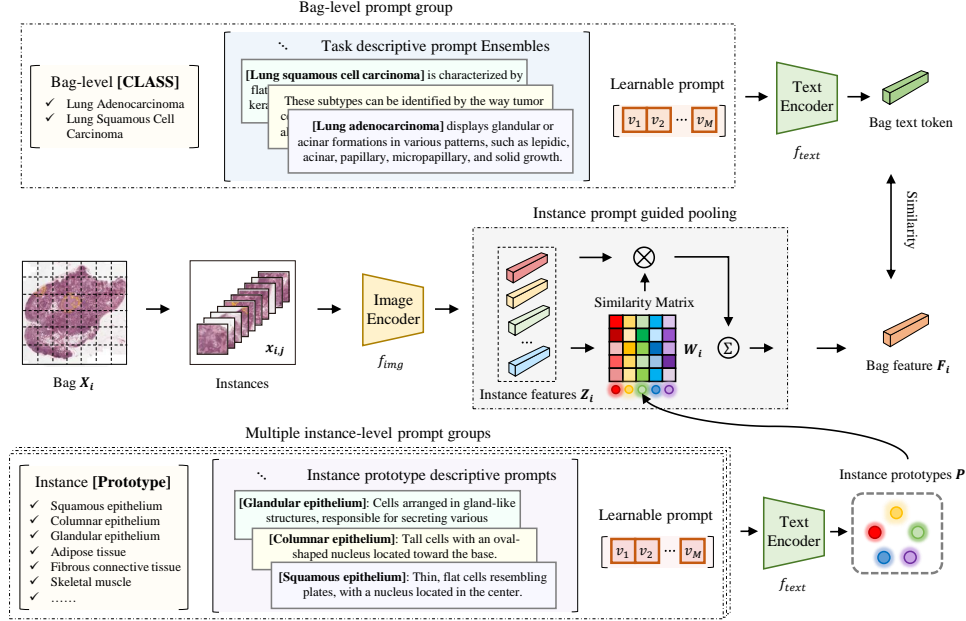


Figure 2: Framework of our proposed TOP.

4 Method

Figure 2 presents our proposed TOP framework. First, we use the Image Encoder f_{img} of CLIP to extract instance features Z_i for all instances within a bag X_i . Then, we propose instance prompt guided pooling to aggregate these instance features into a bag feature F_i . During this process, we use a large language model GPT-4 to generate multiple instance-level prompt groups and input them into the Text Encoder f_{text} of CLIP to generate instance prototypes P , which serve as instance-level language priors to guide the aggregation process. Next, we use GPT-4 to construct a bag-level prompt group and input it into the Text Encoder f_{text} to generate a Bag text token B_i . We then match B_i with the aggregated bag feature F_i to complete bag-level few-shot prompt learning. During this process, the bag-level prompt group serves as a bag-level language prior to guide the few-shot prompt learning process. The loss function for few-shot prompt learning is shown in equation 4 in Section 3.2, and the overall training objective is to use a small amount of bag-level labeled data to optimize the learnable prompt vectors $[V]_m$ in the bag-level and instance-level prompt groups (the two $[V]_m$ vectors are different). In addition, during training, we also constrain the minimum correlation between each Instance prototype in P to prevent all prototypes from being too similar and causing degradation. The construction of instance and bag-level prompts will be introduced in Section 4.1 and the instance prompt guided pooling method will be introduced in Section 4.2.

During inference, for bag classification, we calculate the matching degree between the image features and all target class bag prompt features to determine the classification category, as shown in equation 2 in Section 3.2. For instance classification, we obtain the classification score of each instance by averaging the similarity weights established between each instance feature and multiple text-based instance prototypes.

4.1 Construction of Instance and Bag-level Prompts

We utilize the large language model GPT-4 [24] to construct instance and bag-level prompts as efficient language priors to guide the instance-level feature aggregation and the bag-level few-shot prompt learning.

Instance-level prompt groups are designed to generate visual descriptions of various instance phenotypes as prior knowledge to effectively guide instance-level feature aggregation. Each prompt group corresponds to a potential tissue phenotype that may appear in WSIs and consists of three parts. The first part is a text description of various instance phenotypes in the form of "an image patch of [Lymphocytes]". Typically, instances in a WSI contain information about different phenotypes,

such as different forms of tumor cells, lymphocytes, epithelial cells, etc. For the second part, we used a question-answering mode with GPT-4 to obtain common visual descriptions of different instance phenotypes in WSIs. Note that these visual descriptions do not require manual design but are obtained from GPT-4. Representative instance prototype descriptive prompts of different tasks are shown in Figure 3, 4 and 5. Please note that the construction of instance prototype descriptive prompts depends on the specific task. For example, in the tasks of tumor detection (Camelyon16 Dataset) and lung cancer subtyping (TCGA Lung Cancer Dataset), since the input slides have not been annotated to distinguish different regions, there may be various tissue phenotypes other than cancer cells. Therefore, we construct instance prototype descriptive prompts based on the descriptions corresponding to different tissue phenotypes. On the other hand, in the task of determining lymph node metastasis from primary lesions (Cervical Cancer Dataset), as the network input consists of pre-annotated tumor regions, our focus is mainly on different phenotypic information related to tumor cells when constructing instance prototype descriptive prompts. These descriptions provide medical prior information from different perspectives on the factors leading to high and low probability of lymph node metastasis. For each instance phenotype, we focus on guiding GPT-4 to describe the visual characteristics it has from a visual perspective, thereby establishing visual priors for these phenotypes. Inspired by the learnable prompt in CoOp [42], we design the third part as a learnable prompt representation.

The bag-level prompt group is designed to guide the few-shot prompt learning process at the bag level. It also consists of three parts. The first part is the description of the task label at the bag level in the form of "a WSI of [Lung adenocarcinoma]". The second part is a combination of various visual descriptions for this task label, which are also obtained from GPT-4, as shown in Figure 6 and 7. For each WSI classification task, we guide the GPT-4 model to describe the complex medical concept from a visual perspective, so as to establish a visual prior for the complex medical concept from the textual description. The third part is also designed as a learnable prompt representation.

All detailed bag-level and instance-level task descriptive prompt ensembles will be fully open-source.

4.2 Instance Prompt Guided Pooling

We propose a prompt guided pooling strategy to aggregate instance features into bag features. The main idea is to first calculate similarity weights between the image features of each instance and the prototypes of multiple text descriptions, and then use the weighted average of all instance features in a bag as the bag feature.

Mathematically, assuming that \mathbf{X}_i represents the current bag containing n_i instances, we use the Image Encoder f_{img} to extract instance features $\mathbf{Z}_i \in \mathbb{R}^{n_i \times m}$, where m represents the dimension of the features.

$$\mathbf{Z}_i = f_{img}(\mathbf{X}_i) \quad (5)$$

Then, we input multiple instance-level prompt groups \mathbf{T} into the Text Encoder f_{text} to obtain multiple instance prototypes, $\mathbf{P} \in \mathbb{R}^{n_p \times m}$, where n_p represents the number of prototypes, which corresponds to the number of instance-level prompt groups. It varies depending on the specific classification task.

$$\mathbf{P} = f_{text}(\mathbf{T}) \quad (6)$$

Next, we calculate the dot product of instance features \mathbf{Z}_i and a set of prototypes \mathbf{P} , and then perform softmax normalization by column (each column corresponds to a prototype), obtaining aggregation weights $\mathbf{W}_i \in \mathbb{R}^{n_i \times n_p}$ for each prototype with respect to the current bag. Next, we use the aggregation weights to obtain a set of weighted features $\mathbf{W}_i^\top \cdot \mathbf{Z}_i \in \mathbb{R}^{n_p \times m}$, and finally average the weights of all prototypes to obtain the bag feature $\mathbf{F}_i \in \mathbb{R}^{1 \times m}$.

$$\mathbf{W}_i = \text{Softmax}(\mathbf{Z}_i \cdot \mathbf{P}^\top) \quad (7)$$


$$\mathbf{F}_i = \text{mean}(\mathbf{W}_i^\top \cdot \mathbf{Z}_i) \quad (8)$$

In addition, during training, we also constrain the minimum correlation between each instance prototype in \mathbf{P} to avoid degeneration, which means that all prototypes are too similar to each other, with the following loss:

$$\text{Loss} = \min(\mathbf{W}^\top \times \mathbf{W}) \quad (9)$$

Kindly enumerate common tissues in histological specimens and provide comprehensive descriptions of the characteristics of each type of tissue.

Formatting the responses as **{tissue type} - {description of characteristics}** will help to ensure clarity and organization.

GPT-4  ↓

Epithelial tissue.

This tissue type is characterized by tightly packed cells that form a continuous layer covering body surfaces, lining cavities, and forming glands. It functions as a barrier, protecting the body from pathogens and water loss, and has roles in secretion, absorption, and sensory reception. Epithelial tissue is divided into simple and stratified types, based on the number of layers, and squamous, cuboidal, and columnar types, based on cell shape.

Connective tissue.

Composed of cells, fibers, and an extracellular matrix, connective tissue serves to support, bind, and protect other tissues and organs. It includes a diverse group of tissue types, such as loose connective tissue, dense connective tissue, adipose tissue, cartilage, bone, and blood. Characteristics include varying degrees of vascularity, a range of cell types (e.g., fibroblasts, adipocytes, chondrocytes), and fibers (e.g., collagen, elastin, reticular).

Muscle tissue.

This tissue type is characterized by its contractile nature, which enables movement, maintenance of posture, and heat production. Muscle tissue is classified into three types: skeletal, smooth, and cardiac. Skeletal muscle is striated, voluntary, and attaches to bones; smooth muscle is non-striated, involuntary, and found in the walls of hollow organs; and cardiac muscle is striated, involuntary, and found only in the heart.

Nervous tissue.

Comprised primarily of neurons and supporting cells called neuroglia, nervous tissue is responsible for transmitting electrical signals and processing information within the body. Neurons possess specialized structures, such as dendrites, axons, and cell bodies, to facilitate communication. Neuroglia provide structural support, insulation, and protection to neurons.

Lung Adenocarcinoma.

A subtype of non-small cell lung cancer, lung adenocarcinoma is characterized by the presence of glandular structures, mucin production, and lepidic growth patterns. It often originates in the peripheral regions of the lung and is the most common type of lung cancer in non-smokers.


Lung Squamous Cell Carcinoma.

Another subtype of non-small cell lung cancer, lung squamous cell carcinoma arises from the squamous epithelial cells lining the bronchi. It is characterized by the presence of keratinization, intercellular bridges, and large, polygonal-shaped cells. This type of lung cancer is strongly associated with smoking and typically arises in the central regions of the lung.

.....

Figure 3: Representative instance prototype descriptive prompts for the tasks of tumor detection (Camelyon16 Dataset) and lung cancer subtyping (TCGA Lung Cancer Dataset). Here, only six typical prompts are listed, but in reality, we utilized a total of 26 prompts.

Please provide a summary of the factors found in primary tumor whole slide images that may indicate **{a higher probability of metastasis}**, along with a description of their image features.

GPT-4  ↓

Tumor grade:

The tumor grade is determined by the degree of abnormality of the cancer cells and their arrangement within the tissue. In whole slide images, higher grade tumors display more disorganized and irregular cell patterns, with increased nuclear atypia (abnormal size and shape of cell nuclei) and a higher mitotic rate (increased number of dividing cells).

Tumor size:

The size of the primary tumor can be determined by examining the whole slide image. Larger tumors can be seen occupying a more significant portion of the tissue sample and are generally associated with a higher risk of metastasis.

Lymphovascular invasion (LVI):

In whole slide images, LVI is observed as cancer cells within the lumens of lymphatic or blood vessels. This can appear as clusters or single cells within the vessel walls or channels, suggesting that cancer cells have penetrated these channels, increasing the likelihood of metastasis.

Tumor margins:

Tumor margins refer to the edges of the tumor tissue in the whole slide image. Infiltrative or poorly defined margins can appear as irregular, jagged, or intermingled with surrounding healthy tissue, which may suggest a higher risk of cancer cells breaking away and potentially leading to metastasis.

Inflammatory response and stromal reaction:

In whole slide images, an intense inflammatory response can be seen as an accumulation of immune cells (such as lymphocytes) around the tumor, while a strong stromal reaction is characterized by an increased density and disorganization of the connective tissue surrounding the tumor. Both of these features may be associated with a more aggressive tumor and an increased risk of metastasis.

.....

Figure 4: Representative instance prototype descriptive prompts for the task of determining lymph node metastasis from primary lesions (Cervical Cancer Dataset). Here, only five typical prompts with a higher probability of metastasis are listed, but in reality, we utilized a total of 26 prompts.

5 Experiment

5.1 Datasets

We comprehensively evaluated the instance classification and bag classification performance of TOP in FSWC tasks using three real-world datasets of different cancer types from different centers: the Camelyon 16 Dataset [2] for breast cancer, the TCGA-Lung Cancer Dataset² for lung cancer, and an in-house Cervical Cancer Dataset for cervical cancer.


5.1.1 Camelyon16 Dataset

The publicly available Camelyon16 dataset is a valuable resource for the detection of breast cancer metastasis in lymph nodes [2]. It comprises 400 H&E-stained Whole Slide Images (WSIs) of lymph nodes, with 270 WSIs allocated for training and 130 for testing. WSIs that exhibit metastasis are labeled as positive, whereas those without metastasis are categorized as negative. Importantly, this dataset provides both slide-level labels indicating the overall positivity or negativity of a WSI, as well as pixel-level labels that precisely identify the specific areas of metastasis.

In the weakly supervised scenario studied in this paper, our training process relied only on slide-level labels. To evaluate the instance classification performance of each algorithm, we utilized pixel-level

²<http://www.cancer.gov/tcga>

Please provide a summary of the factors found in primary tumor whole slide images that may indicate { **a lower probability of metastasis** }, along with a description of their image features.

GPT-4  ↓

Well-differentiated tumor cells:

Well-differentiated tumor cells exhibit a more organized and differentiated appearance compared to poorly differentiated cells. This can be observed through distinct cell borders, regular nuclear shape and size, and a lower nuclear-to-cytoplasmic ratio.

Low mitotic activity:

Low mitotic activity refers to a reduced number of cells undergoing division. In whole slide images, this can be identified by a lower density of cells in the mitotic phase, with fewer visible mitotic figures such as condensed chromosomes or spindles.

Intact basement membrane:

The presence of an intact basement membrane, which is a thin layer of extracellular matrix surrounding epithelial tissues, is associated with a lower likelihood of metastasis. This can be identified in whole slide images by a continuous and uninterrupted boundary between tumor cells and the surrounding stroma.

Lack of vascular invasion:

Vascular invasion refers to the infiltration of tumor cells into blood or lymphatic vessels. The absence of vascular invasion can be observed in whole slide images by the absence of tumor cells within the lumen of blood vessels or lymphatic channels.

Minimal stromal reaction:

A minimal stromal reaction indicates limited inflammation or fibrosis in the surrounding tissue. In whole slide images, this can be characterized by a low density of inflammatory cells, absence of fibrotic areas, and limited deposition of extracellular matrix components.

.....

Figure 5: Representative instance prototype descriptive prompts for the task of determining lymph node metastasis from primary lesions (Cervical Cancer Dataset). Here, only five typical prompts with a lower probability of metastasis are listed, but in reality, we utilized a total of 26 prompts.

Please provide the characteristics of WSIs of { **Lung Adenocarcinoma** }?

Please provide the characteristics of WSIs of { **Lung Squamous Cell Carcinoma** }?

GPT-4  ↓

Lung Adenocarcinoma - A subtype of non-small cell lung cancer, lung adenocarcinoma is characterized by the presence of glandular structures, mucin production, and lepidic growth patterns.

Lung Squamous Cell Carcinoma - Another subtype of non-small cell lung cancer. It is characterized by the presence of keratinization, intercellular bridges, and large, polygonal-shaped cells.

Figure 6: Representative bag descriptive prompts for the task of lung cancer subtyping (TCGA Lung Cancer Dataset).

Please provide the characteristics of WSIs with a {**higher risk of metastasis**} from the primary lesion.

Please provide the characteristics of WSIs with a {**lower risk of metastasis**} from the primary lesion.

GPT-4  ↓

Higher risk of metastasis can be suggested by image features such as a high tumor grade with abnormal cell patterns, larger tumor size, presence of lymphovascular invasion, infiltrative tumor margins, and intense inflammatory response and stromal reaction.

Lower risk of metastasis is characterized by well-organized cell patterns with low nuclear atypia, smaller tumor size, absence of lymphovascular invasion, well-defined tumor margins, and mild inflammatory response and stromal reaction.

Figure 7: Representative bag descriptive prompts for the task of determining lymph node metastasis from primary lesions (Cervical Cancer Dataset).

labels of cancerous regions in the test set. Similar to the preprocessing in [16, 27], prior to the training process, we partitioned each WSI into non-overlapping image patches, each measuring 512×512 pixels at a $10\times$ magnification. Patches exhibiting an entropy value lower than 5 were discarded as background noise. Additionally, a patch was considered positive if it encompassed 25% or more cancerous areas; otherwise, it was assigned a negative label. As a result, we obtained a total of 186,604 instances for further analysis.

5.1.2 TCGA Lung Cancer Dataset

The TCGA Lung Cancer dataset, which can be accessed through The Cancer Genome Atlas (TCGA) Data Portal, comprises 1054 WSIs. This dataset specifically targets two distinct subtypes of lung cancer: Lung Adenocarcinoma and Lung Squamous Cell Carcinoma. Our primary goal is to achieve precise diagnoses for both subtypes. In this context, WSIs depicting Lung Adenocarcinoma are categorized as negative, while those showcasing Lung Squamous Cell Carcinoma are classified as positive.

It is worth emphasizing that the provided dataset only includes slide-level labels, and patch-level labels are not accessible. Similar to the preprocessing in [16, 27], at a magnification of $20\times$, the dataset consists of approximately 5.2 million patches, averaging around 5,000 patches per slide. To facilitate the dataset partitioning, 840 slides were allocated for training, while 210 slides were reserved for testing. It is important to note that four slides exhibiting low quality or corruption were excluded from the dataset.

5.1.3 Cervical Cancer Dataset

The Cervical Cancer dataset comprises an in-house clinical pathology dataset containing 374 H&E-stained WSIs of primary lesions of cervical cancer obtained from distinct patients, subsequent to slide selection. All patients underwent abdominal hysterectomy with pelvic lymph node dissection \pm para-aortic lymph node dissection. Following the surgical procedure, the lymph node status of each patient was determined by experienced gynecological pathologists. Moreover, all patients possess meticulous follow-up records spanning over a period exceeding five years, along with the outcomes of major immunohistochemical marker detection. We employed this dataset to accomplish the task of predicting lymph node metastasis from primary lesions, which cannot be directly ascertained by physicians through the examination of H&E-stained slides.

The utilization of deep learning technology holds significant clinical implications in predicting the mentioned clinical task directly from H&E-stained slides. By conducting automated analysis on H&E-stained slides from cervical cancer patients, it becomes feasible to effectively predict lymph node metastasis in primary lesions prior to treatment. This predictive capability aids in the selection of suitable treatment plans and personalized therapies.

Table 1: Performance of bag-level classification on the Camelyon 16 Dataset.

Method	16-shot	8-shot	4-shot	2-shot	1-shot
Linear-Probe (Mean-pooling)	0.5273	0.5631	0.4828	0.3160	0.3325
Linear-Probe (Max-pooling)	0.5847	0.5789	0.5352	0.5319	0.5298
Linear-Probe (Attention-pooling)	0.7794	0.6991	0.6817	0.6255	0.5298
CoOp (Attention-pooling)	0.8088	0.6799	0.6604	0.6568	0.6500
Instance+Bag Prompt Learning (Ours)	0.8303	0.7266	0.7167	0.6967	0.6714

Table 2: Performance of instance-level classification on the Camelyon 16 Dataset.

Method	16-shot	8-shot	4-shot	2-shot	1-shot
Linear-Probe (Attention-pooling)	0.7521	0.6766	0.6564	0.6444	0.6283
CoOp (Attention-pooling)	0.8528	0.6624	0.6316	0.6206	0.5975
Instance+Bag Prompt Learning (Ours)	0.8923	0.7270	0.7120	0.7035	0.6977

Similar to the preprocessing in [27], the experiment was conducted at a magnification of $5\times$, and each WSI was partitioned into non-overlapping patches of size 224×224 to form a bag. Background patches with entropy values below 5 were excluded from the original WSI. The slides corresponding to patients who experienced pelvic lymph node metastasis were labeled as positive (209 cases), while those who did not develop pelvic lymph node metastasis were labeled as negative (165 cases). The WSIs were randomly divided into a training set (300 cases) and a test set (74 cases).

5.2 Evaluation Metrics and Comparison Methods

For both instance and bag classification, we use Area Under Curve (AUC) as the evaluation metric. However, it should be noted that only the Camelyon 16 Dataset has the true labels for each instance, while the other two datasets only have bag-level labels. Therefore, we evaluate the instance and bag classification performance of each method on the Camelyon 16 Dataset, and only evaluate the bag classification performance on the latter two datasets.

Because existing few-shot learning methods cannot be used in FSWC task, we constructed four baselines based on the current state-of-the-art few-shot learning methods CoOp [42] and Linear Probe [28]: (1) Linear-Probe (Mean pooling), (2) Linear-Probe (Max pooling), (3) Linear-Probe (Attention pooling), and (4) CoOp (Attention pooling). Specifically, we first used CLIP as the image feature extractor to extract all instance features within each bag. Then, we aggregated all instance features within a bag using simple Mean, Max pooling or learnable Attention Pooling [13] to obtain the bag feature. Linear-Probe indicates that we used a linear layer to perform bag-level classification on the aggregated bag feature. CoOp indicates that we used the bag-level label and learnable prompt to perform bag-level classification through prompt learning. We conducted few-shot classification experiments with 1, 2, 4, 8, and 16 labeled bags for each class.

5.3 Implementation Details

We used the image encoder and text encoder of CLIP as the feature extractors for both images and text. The number of learnable parameters is set to 10 tokens for both instance and bag prompt. During training, we fixed all weights of CLIP and only trained the learnable parameters of bag prompt and instance prompt. Unlike general few-shot scenarios, few-shot weakly-supervised learning is a very challenging setting. When the randomly selected bags have poor representativeness, the network usually struggles to learn meaningful results. Therefore, for experiments with different shots, we randomly trained the network five times with different labeled bags and reported the highest performance of each method.

5.4 Results on the Camelyon 16 Dataset

The bag classification and instance classification performance on the Camelyon 16 dataset are shown in Tables 1 and 2, respectively. It can be seen that TOP achieved the best bag and instance classification performance in all few-shot settings, and significantly outperformed all comparison methods by a large margin. It can be observed that Linear-Probe with Mean/Max pooling can hardly work. Although using trainable attention pooling helps learn the importance of each instance and improves the performance of Linear-Probe, it still has limitations in performance. Prompt learning with fully trainable prompts in CoOp outperforms Linear-Probe. In contrast, our method used a two-level prompt learning paradigm, which achieved the best performance on both bag and instance

Table 3: Performance of bag-level classification on the TCGA-Lung Cancer Dataset.

Method	16-shot	8-shot	4-shot	2-shot	1-shot
Linear-Probe (Mean-pooling)	0.6533	0.5389	0.4485	0.5293	0.4534
Linear-Probe (Max-pooling)	0.4848	0.4955	0.4422	0.4839	0.4903
Linear-Probe (Attention-pooling)	0.7250	0.6579	0.6247	0.5836	0.5623
CoOp (Attention-pooling)	0.7835	0.6799	0.6760	0.6754	0.6781
Instance+Bag Prompt-Learning (Ours)	0.8206	0.8051	0.7541	0.7238	0.7101

Table 4: Performance of bag-level classification on the Cervical Cancer Dataset.

Method	16-shot	8-shot	4-shot	2-shot	1-shot
Linear-Probe (Mean-pooling)	0.6756	0.6511	0.6611	0.6656	0.6511
Linear-Probe (Max-pooling)	0.3833	0.6200	0.6011	0.5878	0.5878
Linear-Probe (Attention-pooling)	0.8000	0.7400	0.7533	0.6900	0.5222
CoOp (Attention-pooling)	0.6994	0.6800	0.6756	0.6954	0.6544
Instance+Bag Prompt-Learning (Ours)	0.8233	0.8024	0.7889	0.7622	0.7044

classification, with an average improvement of 3.7% and 7.3%, respectively, over the second-best method.

5.5 Results on the TCGA-Lung Cancer Dataset and the Cervical Cancer Dataset

The results on the TCGA-Lung Cancer Dataset are shown in Table 3. It can be seen that TOP still achieves the best bag classification performance in all few-shot settings, and significantly outperforms all competitors by a large margin, with an average improvement of 6.4% over the second-best method.

The results on the Cervical Cancer Dataset are shown in Table 4. It should be noted that this task is extremely challenging, and even pathologists cannot make direct judgments. TOP displays strongest performance, with an average improvement of 7.5% over the second-best method.

Table 5: Ablation results of bag-level classification on the Camelyon 16 Dataset.

Method	16-shot	8-shot	4-shot	2-shot	1-shot
Bag Prompt+Attention-pooling	0.8135	0.6930	0.6740	0.6616	0.6527
CoOp+Attention-pooling	0.8088	0.6799	0.6604	0.6568	0.6500
CoOp+Prompt guided pooling	0.8207	0.7032	0.6865	0.6714	0.6636
Bag Prompt+Prompt guided pooling (Ours)	0.8303	0.7266	0.7167	0.6967	0.6714

Table 6: Ablation results of instance-level classification on the Camelyon 16 Dataset.

Method	16-shot	8-shot	4-shot	2-shot	1-shot
Bag Prompt+Attention-pooling	0.8687	0.6716	0.6407	0.6254	0.5993
CoOp+Attention-pooling	0.8528	0.6624	0.6316	0.6206	0.5975
CoOp+Prompt guided pooling	0.8793	0.6899	0.6502	0.6356	0.6038
Bag Prompt+Prompt guided pooling (Ours)	0.8923	0.7270	0.7120	0.7035	0.6977

6 Ablation Study

We conducted ablation experiments on the two key components of TOP, the instance prompt guided pooling and bag-level prompt group. Experiments are conducted on the Camelyon 16 Dataset, and the bag classification and instance classification results are shown in Table 5 and Table 6, respectively. In the two tables, "Prompt guided pooling" represents the use of our proposed instance prompt guided aggregation method while "Attention-pooling" represents the use of attention-based method to aggregate instance features into bag features; "Bag Prompt" represents the use of our proposed Bag-level prompt group while "CoOp" represents using only the learnable part and bag labels as prompt at the bag-level prompt learning.

Effectiveness of instance prompt guided pooling. In both Table 5 and Table 6, no matter 'Bag Prompt' or 'CoOp' is used for the bag-level prompt learning, 'Prompt guided pooling' consistently results in significantly better performance than 'Attention pooling', which indicates the effectiveness of our proposed Prompt guided pooling strategy for instance feature aggregation.

Effectiveness of Bag-level prompt group. In Table 5 and Table 6, no matter what instance feature aggregation method is used, 'Bag-prompt' always outperforms 'CoOp', which indicates that our proposed Task descriptive prompt is better than current SOTA methods of fully learnable prompt.

7 Algorithm Stability with Different Shots

Unlike general few-shot scenarios, few-shot weakly supervised WSI classification is a very challenging setting. When the randomly selected bags have poor representativeness, the network usually struggles to learn meaningful results. Therefore, for experiments with different shots, we randomly trained the network five times with different labeled bags and reported the highest performance of each method. We further demonstrate the stability of our method under different shots. We ran our method five times on 1, 2, 4, 8, and 16 shots, and recorded the Standard Deviation (STD) of bag AUC and instance AUC, as shown in Figure 8. From the figure, it can be observed that the algorithm exhibits instability when there are too few support bags, which is understandable in the highly challenging few-shot weakly supervised classification (FSWC) task. However, as the number of shots increases, the performance of our method gradually becomes stable.

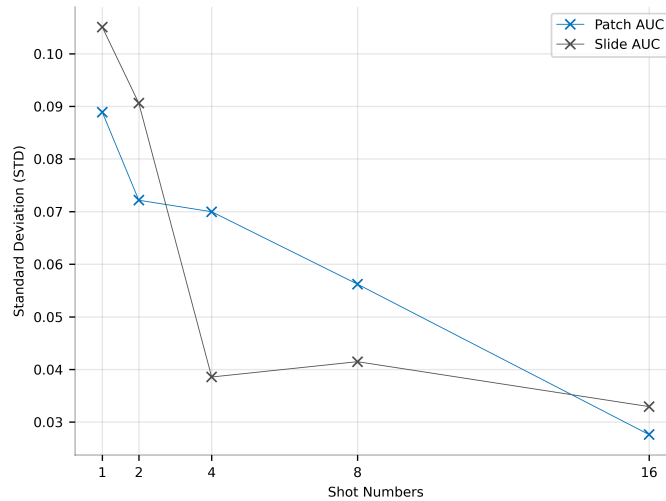


Figure 8: Algorithm stability with different shots.

8 Conclusion

In this paper, we introduce the novel problem of Few-shot Weakly-supervised WSI Classification (FSWC) for the first time. We proposed a Two-level Prompt Learning MIL framework named TOP to solve the FSWC problem effectively. TOP utilizes GPT-4 to generate both instance-level and bag-level visual descriptions to facilitate instance feature aggregation and bag-level prompt learning. Experiments on three WSI classification tasks shows the high performance of TOP in FSWC tasks. However, this paper has certain limitations, mainly due to the effectiveness of the proposed prompt depending on the capabilities of the large model. If the large model fails to provide effective descriptions, it can affect the model’s performance. This study aims to inspire further research that combines foundational models with large-scale language models for the classification of pathology Whole Slide Images. Such research endeavors will herald a new era in AI pathology.

References

- [1] Peyman Bateni, Raghav Goyal, Vaden Masrani, Frank Wood, and Leonid Sigal. Improved few-shot visual classification. In *Proceedings of the IEEE/CVF Conference on Computer Vision and Pattern Recognition (CVPR)*, pages 14493–14502, 2020.
- [2] Babak Ehteshami Bejnordi, Mitko Veta, Paul Johannes Van Diest, Bram Van Ginneken, Nico Karssemeijer, Geert Litjens, Jeroen AWM Van Der Laak, Meyke Hermsen, Quirine F Manson, Maschenka Balkenhol, et al. Diagnostic assessment of deep learning algorithms for detection of lymph node metastases in women with breast cancer. *JAMA*, 318(22):2199–2210, 2017.

- [3] Gabriele Campanella, Matthew G Hanna, Luke Geneslaw, Allen Miraflor, Vitor Werneck Krauss Silva, Klaus J Busam, Edi Brogi, Victor E Reuter, David S Klimstra, and Thomas J Fuchs. Clinical-grade computational pathology using weakly supervised deep learning on whole slide images. *Nature Medicine*, 25(8):1301–1309, 2019.
- [4] Richard J Chen, Chengkuan Chen, Yicong Li, Tiffany Y Chen, Andrew D Trister, Rahul G Krishnan, and Faisal Mahmood. Scaling vision transformers to gigapixel images via hierarchical self-supervised learning. In *Proceedings of the IEEE/CVF Conference on Computer Vision and Pattern Recognition (CVPR)*, pages 16144–16155, 2022.
- [5] Richard J Chen and Rahul G Krishnan. Self-supervised vision transformers learn visual concepts in histopathology. *arXiv preprint arXiv:2203.00585*, 2022.
- [6] Richard J Chen, Ming Y Lu, Jingwen Wang, Drew FK Williamson, Scott J Rodig, Neal I Lindeman, and Faisal Mahmood. Pathomic fusion: an integrated framework for fusing histopathology and genomic features for cancer diagnosis and prognosis. *IEEE Transactions on Medical Imaging*, 41(4):757–770, 2020.
- [7] Richard J Chen, Ming Y Lu, Wei-Hung Weng, Tiffany Y Chen, Drew FK Williamson, Trevor Manz, Maha Shady, and Faisal Mahmood. Multimodal co-attention transformer for survival prediction in gigapixel whole slide images. In *Proceedings of the IEEE/CVF International Conference on Computer Vision (ICCV)*, pages 4015–4025, 2021.
- [8] Veronika Cheplygina, Marleen de Bruijne, and Josien PW Pluim. Not-so-supervised: a survey of semi-supervised, multi-instance, and transfer learning in medical image analysis. *Medical Image Analysis*, 54:280–296, 2019.
- [9] Philip Chikontwe, Meejeong Kim, Soo Jeong Nam, Heounjeong Go, and Sang Hyun Park. Multiple instance learning with center embeddings for histopathology classification. In *Medical Image Computing and Computer Assisted Intervention (MICCAI)*, pages 519–528. Springer, 2020.
- [10] Chelsea Finn, Pieter Abbeel, and Sergey Levine. Model-agnostic meta-learning for fast adaptation of deep networks. In *International Conference on Machine Learning (ICML)*, pages 1126–1135. PMLR, 2017.
- [11] Chelsea Finn, Kelvin Xu, and Sergey Levine. Probabilistic model-agnostic meta-learning. *Advances in Neural Information Processing Systems (NeurIPS)*, 31, 2018.
- [12] Noriaki Hashimoto, Daisuke Fukushima, Ryoichi Koga, Yusuke Takagi, Kaho Ko, Kei Kohno, Masato Nakaguro, Shigeo Nakamura, Hidekata Hontani, and Ichiro Takeuchi. Multi-scale domain-adversarial multiple-instance cnn for cancer subtype classification with unannotated histopathological images. In *Proceedings of the IEEE/CVF Conference on Computer Vision and Pattern Recognition (CVPR)*, pages 3852–3861, 2020.
- [13] Maximilian Ilse, Jakub Tomczak, and Max Welling. Attention-based deep multiple instance learning. In *International Conference on Machine Learning (ICML)*, pages 2127–2136. PMLR, 2018.
- [14] Chao Jia, Yinfei Yang, Ye Xia, Yi-Ting Chen, Zarana Parekh, Hieu Pham, Quoc Le, Yun-Hsuan Sung, Zhen Li, and Tom Duerig. Scaling up visual and vision-language representation learning with noisy text supervision. In *International Conference on Machine Learning (ICML)*, pages 4904–4916. PMLR, 2021.
- [15] Fahdi Kanavati, Gouji Toyokawa, Seiya Momosaki, Michael Rambeau, Yuka Kozuma, Fumihiro Shoji, Koji Yamazaki, Sadanori Takeo, Osamu Iizuka, and Masayuki Tsuneki. Weakly-supervised learning for lung carcinoma classification using deep learning. *Scientific Reports*, 10(1):9297, 2020.
- [16] Bin Li, Yin Li, and Kevin W Eliceiri. Dual-stream multiple instance learning network for whole slide image classification with self-supervised contrastive learning. In *Proceedings of the IEEE/CVF Conference on Computer Vision and Pattern Recognition (CVPR)*, pages 14318–14328, 2021.

- [17] Tiancheng Lin, Hongteng Xu, Canqian Yang, and Yi Xu. Interventional multi-instance learning with deconfounded instance-level prediction. In *Proceedings of the AAAI Conference on Artificial Intelligence (AAAI)*, volume 36, pages 1601–1609, 2022.
- [18] Tiancheng Lin, Zhimiao Yu, Hongyu Hu, Yi Xu, and Chang Wen Chen. Interventional bag multi-instance learning on whole-slide pathological images. *arXiv preprint arXiv:2303.06873*, 2023.
- [19] Ming Y Lu, Richard J Chen, Dehan Kong, Jana Lipkova, Rajendra Singh, Drew FK Williamson, Tiffany Y Chen, and Faisal Mahmood. Federated learning for computational pathology on gigapixel whole slide images. *Medical Image Analysis*, 76:102298, 2022.
- [20] Ming Y Lu, Richard J Chen, Jingwen Wang, Debora Dillon, and Faisal Mahmood. Semi-supervised histology classification using deep multiple instance learning and contrastive predictive coding. *arXiv preprint arXiv:1910.10825*, 2019.
- [21] Ming Y Lu, Tiffany Y Chen, Drew FK Williamson, Melissa Zhao, Maha Shady, Jana Lipkova, and Faisal Mahmood. Ai-based pathology predicts origins for cancers of unknown primary. *Nature*, 594(7861):106–110, 2021.
- [22] Ming Y Lu, Drew FK Williamson, Tiffany Y Chen, Richard J Chen, Matteo Barbieri, and Faisal Mahmood. Data-efficient and weakly supervised computational pathology on whole-slide images. *Nature Biomedical Engineering*, 5(6):555–570, 2021.
- [23] Faisal Mahmood, Daniel Borders, Richard J Chen, Gregory N McKay, Kevan J Salimian, Alexander Baras, and Nicholas J Durr. Deep adversarial training for multi-organ nuclei segmentation in histopathology images. *IEEE Transactions on Medical Imaging*, 39(11):3257–3267, 2019.
- [24] OpenAI. Gpt-4 technical report. *arXiv preprint arXiv:2303.08774*, 2023.
- [25] Linhao Qu, Siyu Liu, Xiaoyu Liu, Manning Wang, and Zhijian Song. Towards label-efficient automatic diagnosis and analysis: a comprehensive survey of advanced deep learning-based weakly-supervised, semi-supervised and self-supervised techniques in histopathological image analysis. *Physics in Medicine & Biology*, 2022.
- [26] Linhao Qu, Xiaoyuan Luo, Shaolei Liu, Manning Wang, and Zhijian Song. Dgmil: Distribution guided multiple instance learning for whole slide image classification. In *Medical Image Computing and Computer Assisted Intervention (MICCAI)*, pages 24–34. Springer, 2022.
- [27] Linhao Qu, Xiaoyuan Luo, Manning Wang, and Zhijian Song. Bi-directional weakly supervised knowledge distillation for whole slide image classification. *Advances in Neural Information Processing Systems (NeurIPS)*, 35:15368–15381, 2022.
- [28] Alec Radford, Jong Wook Kim, Chris Hallacy, Aditya Ramesh, Gabriel Goh, Sandhini Agarwal, Girish Sastry, Amanda Askell, Pamela Mishkin, Jack Clark, et al. Learning transferable visual models from natural language supervision. In *International Conference on Machine Learning (ICML)*, pages 8748–8763. PMLR, 2021.
- [29] Jérôme Rony, Soufiane Belharbi, Jose Dolz, Ismail Ben Ayed, Luke McCaffrey, and Eric Granger. Deep weakly-supervised learning methods for classification and localization in histology images: a survey. *arXiv preprint arXiv:1909.03354*, 2019.
- [30] Zhuchen Shao, Hao Bian, Yang Chen, Yifeng Wang, Jian Zhang, Xiangyang Ji, et al. Transmil: Transformer based correlated multiple instance learning for whole slide image classification. *Advances in Neural Information Processing Systems (NeurIPS)*, 34:2136–2147, 2021.
- [31] Xiaoshuang Shi, Fuyong Xing, Yuanpu Xie, Zizhao Zhang, Lei Cui, and Lin Yang. Loss-based attention for deep multiple instance learning. In *Proceedings of the AAAI Conference on Artificial Intelligence (AAAI)*, volume 34, pages 5742–5749, 2020.
- [32] Jake Snell, Kevin Swersky, and Richard Zemel. Prototypical networks for few-shot learning. *Advances in Neural Information Processing Systems (NeurIPS)*, 30, 2017.

- [33] Chetan L Srinidhi, Ozan Ciga, and Anne L Martel. Deep neural network models for computational histopathology: A survey. *Medical Image Analysis*, 67:101813, 2021.
- [34] Flood Sung, Yongxin Yang, Li Zhang, Tao Xiang, Philip HS Torr, and Timothy M Hospedales. Learning to compare: Relation network for few-shot learning. In *Proceedings of the IEEE Conference on Computer Vision and Pattern Recognition (CVPR)*, pages 1199–1208, 2018.
- [35] Chao Tu, Yu Zhang, and Zhenyuan Ning. Dual-curriculum contrastive multi-instance learning for cancer prognosis analysis with whole slide images. *Advances in Neural Information Processing Systems (NeurIPS)*, 35:29484–29497, 2022.
- [36] Oriol Vinyals, Charles Blundell, Timothy Lillicrap, Daan Wierstra, et al. Matching networks for one shot learning. *Advances in Neural Information Processing Systems (NeurIPS)*, 29, 2016.
- [37] Xiyue Wang, Jinxi Xiang, Jun Zhang, Sen Yang, Zhongyi Yang, Ming-Hui Wang, Jing Zhang, Wei Yang, Junzhou Huang, and Xiao Han. Scl-wc: Cross-slide contrastive learning for weakly-supervised whole-slide image classification. *Advances in Neural Information Processing Systems (NeurIPS)*, 35:18009–18021, 2022.
- [38] Yongluan Yan, Xinggang Wang, Xiaojie Guo, Jiemin Fang, Wenyu Liu, and Junzhou Huang. Deep multi-instance learning with dynamic pooling. In *Asian Conference on Machine Learning (ACML)*, pages 662–677. PMLR, 2018.
- [39] Jiawen Yao, Xinliang Zhu, Jitendra Jonnagaddala, Nicholas Hawkins, and Junzhou Huang. Whole slide images based cancer survival prediction using attention guided deep multiple instance learning networks. *Medical Image Analysis*, 65:101789, 2020.
- [40] Lewei Yao, Runhui Huang, Lu Hou, Guansong Lu, Minzhe Niu, Hang Xu, Xiaodan Liang, Zhenguo Li, Xin Jiang, and Chunjing Xu. Filip: fine-grained interactive language-image pre-training. *arXiv preprint arXiv:2111.07783*, 2021.
- [41] Hongrun Zhang, Yanda Meng, Yitian Zhao, Yihong Qiao, Xiaoyun Yang, Sarah E Coupland, and Yalin Zheng. Dtf-d-mil: Double-tier feature distillation multiple instance learning for histopathology whole slide image classification. In *Proceedings of the IEEE/CVF Conference on Computer Vision and Pattern Recognition (CVPR)*, pages 18802–18812, 2022.
- [42] Kaiyang Zhou, Jingkang Yang, Chen Change Loy, and Ziwei Liu. Learning to prompt for vision-language models. *International Journal of Computer Vision*, 130(9):2337–2348, 2022.
- [43] Xinliang Zhu, Jiawen Yao, Feiyun Zhu, and Junzhou Huang. Wsisa: Making survival prediction from whole slide histopathological images. In *Proceedings of the IEEE/CVF Conference on Computer Vision and Pattern Recognition (CVPR)*, pages 7234–7242, 2017.